Journal of
Materials Chemistry C

Accepted Manuscript

Cite this: DOI: 10.1039/c0xx00000x

www.rsc.org/xxxxxx

ARTICLE TYPE

Plasmon-Enhanced Catalysis of Photo-Induced Charge Transfer from $TCNQF_4^-$ to $TCNQF_4^{2-}$

Jing Wang,[a] Weiqing Xu,[a] Jinxia Wu,[a] Guangtao Yu,[b] Xianghua Zhou,[a] and Shuping Xu[a]*

Received (in XXX, XXX) Xth XXXXXXXXX 20XX, Accepted Xth XXXXXXXXX 20XX

DOI: 10.1039/b000000x

Ag_2-$TCNQF_4$ ($TCNQF_4$=2,3,5,6-tetrafluoro-7,7,8,8-tetracyanoquinodimethane) was synthesized for the first time via a photo-induced charge transfer of the precursor of semiconductor Ag-$TCNQF_4$ under Au nanoparticles (AuNPs) as a catalyst. We first prepared the one-dimensional Ag-$TCNQF_4$ crystal wires on a solid-supported substrate via the solution process. Then, Ag-$TCNQF_4$ reacted with $KAuCl_4$ via the galvanic replacement reaction to form a metal/semiconductor complex, AuNPs decorated Ag-$TCNQF_4$ (AuNPs@Ag-$TCNQF_4$). The resulted Ag-$TCNQF_4$ crystal wires and AuNPs@Ag-$TCNQF_4$ complex were characterized by scanning electron microscopy (SEM), X-ray diffraction, ultraviolet–visible (UV-vis) and X-ray photoelectron spectroscopies. Under the plasmon-enhanced catalysis of AuNPs, a laser-induced charge transfer process happened on Ag-$TCNQF_4$, varying it to Ag_2-$TCNQF_4$. Time-resolved *in situ* Raman spectra were recorded to monitor the photo-induced charge transfer process. The Raman data show that this photo-induced charge transfer process is laser wavelength-dependant, power-dependant and irradiation time-dependant. It is also affected by the loading of AuNPs. The SEM images, UV-vis and infrared spectra of AuNPs@Ag$TCNQF_4$ before and after laser irradiation further prove that the charge transfer product is Ag_2-$TCNQF_4$. The mechanism of the plasmon-enhanced catalysis of photo-induced charge transfer from $TCNQF_4^-$ to $TCNQF_4^{2-}$ is suggested, which provides a good model to study the charge transfer process in metal/semiconductor systems. In addition, this material has significance for the applications on memory storage and photoelectric devices.

1. Introduction

One-dimensional (1D) metal-organic charge transfer semiconductors, metal-7,7,8,8-tetracyanoquinodimethane (M-TCNQ, while M= Cu^+ or Ag^+), have received an abundance of attention because of their electrical and optical bistable switching behaviors, memory functions, and field emission properties.[1-10] When $TCNQ^-$ is replaced by tetra-fluoride (2,3,5,6-tetrafluoro-7,7,8,8-tetracyanoquinodimethane, $TCNQF_4^-$), the metal-organic semiconductor (M-$TCNQF_4$ while M = Cu^+ or Ag^+) turns into a delocalized electronic structure and the electron affinity raises as well since $TCNQF_4^-$ is a stronger electron acceptor relative to $TCNQ^-$.[11-12] In recent studies, these fluorinated analogues have received renewed attention on their spatial structures, synthesis methods and potential applications.[12, 13, 14] Especially for Ag-$TCNQF_4$, it is regarded as an outstanding candidate for electrical switching devices,[11] field-emission cathodes[15] and catalysts.[16] As early as 1982, Ag-$TCNQF_4$ has been synthesized through a spontaneous redox reaction.[17] Subsequently, its single-crystal structure was obtained.[18] Electron diffraction crystal structure of Ag-$TCNQF_4$ demonstrated that four $TCNQF_4^-$ ions are combined with Ag ions in a tetrahedral environment with a highly distorted configuration.[5] Two independent networks generate a propagating parallel $TCNQF_4^-$ layer, which has a relative orientation angle of 90° with adjacent twofold $TCNQF_4^-$ layers.[5] The strong π-π stacking between Ag-$TCNQF_4$ achieves a 1D column stack nanostructure.[11,13,18] Furthermore, theoretical studies proved that the structure of Ag-$TCNQF_4$ nanowire is the π-π stacking of quadruple $TCNQF_4^-$ around Ag^+.[13]

Many methods have been employed to prepare Ag-$TCNQF_4$. The early synthetic method is spontaneous redox reaction, achieving a Ag-$TCNQF_4$ film on a Ag substrate.[11] The vacuum vapor-solid chemical reaction can obtain wire-typed Ag-$TCNQF_4$.[15] It has also been reported that the direct mix of Ag^+ cations and $TCNQF_4^-$ salt can produce crystallic Ag-$TCNQF_4$ nanowires.[18]

As a typical charge transfer organic semiconductor, the Ag-$TCNQF_4$ can be changed to Ag_2-$TCNQF_4$. In Le's work, they obtained a Ag_2-$TCNQF_4$ film via heating Ag-$TCNQF_4$ in vacuum.[19] Recently, Kotsiliou et al. employed a reduction reaction of $TCNQF_4$ to *in situ* prepare Ag-$TCNQF_4$ and Ag_2-$TCNQF_4$ on an electrode.[14]

In this study, a new, simple and effective route for synthesizing Ag_2-$TCNQF_4$ is proposed. We employed a plasmon-assisted catalytic process to *in situ* transfer $TCNQF_4^-$ to $TCNQF_4^{2-}$ via a photo-induced charge transfer reaction. First, 1D Ag-$TCNQF_4$ crystal wires were prepared on a Ag film modified glass slide by a redox reaction. Then, we modified the 1D Ag-$TCNQF_4$ crystal wires with Au nanoparticles (AuNPs). The photo-induced charge

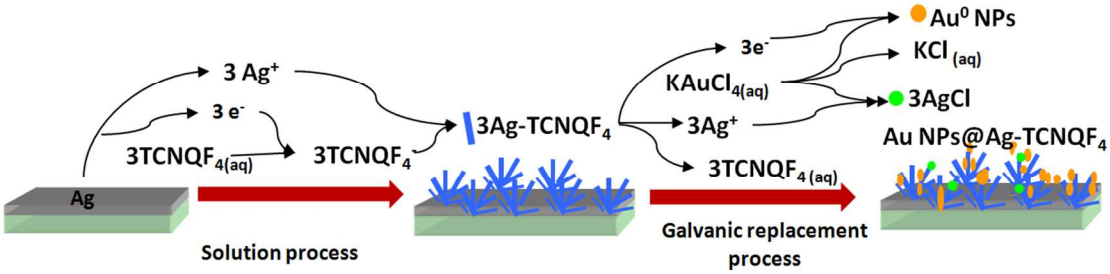

Scheme 1. The strategy for preparing Au nanoparticles-decorated Ag-$TCNQF_4$ complex.

transfer reaction was carried out when the AuNPs decorated Ag-$TCNQF_4$ (AuNPs@Ag-$TCNQF_4$) was exposed to a high energy laser (488, 514, or 532 nm). The localized surface plasmons (LSPs) of AuNPs resonate with light, assisting the photo-induced charge transfer from Ag-$TCNQF_4$, forming Ag_2-$TCNQF_4$. This charge transfer process was monitored and proved via Raman spectroscopy. Impacting factors on the photo-induced charge transfer reaction were discussed, involving the laser wavelength, power density, irradiation time, and the AuNPs loading density. Eventually, the mechanism of photo-induced charge transfer was proposed.

2. Experimental Section

2.1 Chemicals and Materials.

7,7,8,8-tetracyano-2,3,5,6-tetrafluoroquinodimethane ($TCNQF_4$) was obtained from Sigma-Aldrich. Acetonitrile (for HPLC, ≥99.9%) and $KAuCl_4{\cdot}2H_2O$ (Au≥52%) were purchased from Aladdin Company.

2.2 Synthesis of AuNPs@Ag-$TCNQF_4$.

Scheme 1 shows the preparation process of AuNPs@Ag-$TCNQF_4$. First, 1D Ag-$TCNQF_4$ crystal wires were prepared on a clean glass slide via immersing a 100 nm thickness silver film deposited glass slide into a $TCNQF_4$ acetonitrile solution (2.0 mg/mL) at room temperature for two minutes.[20] After that, the 1D wire-shaped Ag-$TCNQF_4$ crystals formed. The residual $TCNQF_4$ was removed by anhydrous acetonitrile. The average length of the Ag-$TCNQF_4$ crystal wires was about 4 μm (statistical result from its SEM image). This process can be descirbed as equation (1):

$$Ag_{(s)} + TCNQF_{4(aq)} \rightarrow Ag\text{-}TCNQF_{4(s)} \quad (1)$$

Then, Ag-$TCNQF_4$ crystal wires were immersed in different concentrations of $KAuCl_4$ acetonitrile solutions (1.0 μM, 10.0 μM, 50,0 μM, 0.1 mM, 0.5 mM, 1.0 mM, 5.0 mM, and 10.0 mM) for one minute. Via a galvanic replacement reaction, AuNPs were formed on the surface of Ag-$TCNQF_4$ crystal wires.[21] This processes can be described by the following equation (2):

$$3Ag\text{-}TCNQF_{4(s)} + K^+[AuCl_4]^-_{(aq)} \rightarrow Au^0_{(s)} + 3TCNQF_4{}^0_{(aq)} + 3AgCl_{(s)} + KCl^-_{(aq)} \quad (2)$$

2.3 Characterization.

Raman spectra were obtained with a Portable MiniRam Raman spectrometer (BWTEK, USA) and microscope utilizing a 785 nm, 2.96 mW excitation source. The Raman spectra excited under 532 nm laser (High-power semiconductor laser BWTEK, USA) were recorded with another Portable BWTEK Raman spectrometer. The diameter of the irradiation spot is about 800 μm. The Raman spectra under 633 nm excitation wavelength were recorded from a LabRam Aramis Raman Microscope system (Horiba-JobinYvon, France) which equipped with an water-cooled He-Ne ion laser as an excitation source. The Raman spectra under 488 and 514 nm excitation wavelengths were obtained on a Jobin Yvon T64000 system (Horiba-JobinYvon, France). Spatial resolution is 2 cm^{-1}, equipped with a water-cooled Ar ion laser as an excitation source. The laser powers reaching to samples were measured by a COHERENT Laser power meter.

Infrared (IR) spectra were measured by a Fourier transform spectrometer (Bruker Vertex 80v) equipped with a liquid nitrogen-cooled mercury cadmiumtelluride (MCT) detector. Scanning electron microscopic (SEM) images of the micro-structures were achieved with HITACHI SU8020 systerm cold field emission scanning electron microscope. Ultraviolet–visible (Uv-vis) spectra were recorded with an Ocean Optics USB4000 spectrometer. X-ray photoelectron spectra (XPS) were carried out using an VG ESCALAB MK II electron spectrometer, the excitation source is Mg Kα X-rays (hν = 1253.6 eV). Powder X-ray diffraction (XRD) patterns of Ag-$TCNQF_4$ and Ag_2-$TCNQF_4$ were performed on a SmartLab Smart powder X-ray diffractometer with Cu KR radiation.

3. Results and discussion

3.1 Characterization of Ag-$TCNQF_4$ and AuNPs@Ag-$TCNQF_4$.

3. 1.1 SEM Characterization.

Figure 1a shows the SEM image of the 1D wire-shaped Ag-$TCNQF_4$ crystals. It can be found the Ag-$TCNQF_4$ crystal wires are prisms in micron-size. Figure 1(b-i) show the SEM images of AuNPs@AgTCNQF$_4$ which were prepared by using increasing concentrations of $KAuCl_4$ acetonitrile solutions via the galvanic replacement reaction. Different concentrations of $KAuCl_4$ acetonitrile solutions cause different morphologies of deposited Au. When the concentration of $KAuCl_4$ was lower than 1.0 μM, only a number of small AuNPs with an average size of 40 nm were attached to the surface of the Ag-$TCNQF_4$ crystals wires (Figure 1b). At the same time, the Ag-$TCNQF_4$ crystal wires were etched into pieces, because part Ag-$TCNQF_4$ wires could be dissolved in acetonitrile solution. When the $KAuCl_4$ concentration was increased to 10 μM (Figure 1c), many mono-disperse rhombic AuNPs (diameter is about 80 nm) formed along the arrises of wires and a few of them were scattered on the surfaces. It is noted that the dissolution of Ag-$TCNQF_4$ crystal

wires reduced. The crystal wires were etched only at the

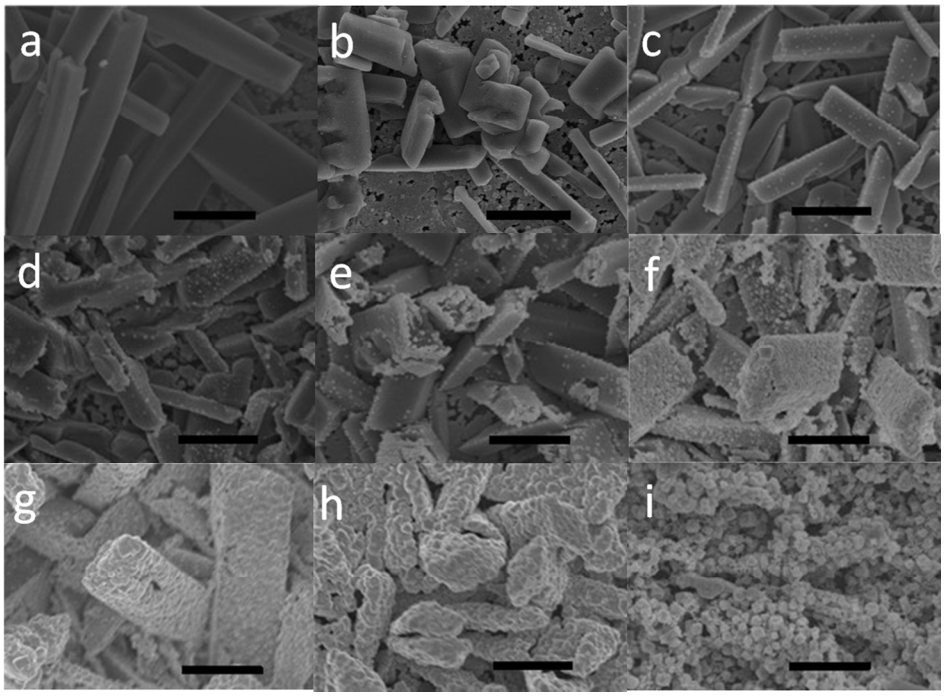

Figure 1. SEM images of a)Ag-TCNQF$_4$ nanowires and AuNPs@Ag-TCNQF$_4$ microrods which were prepared by using b) 1.0 μM, c) 10.0 μM, d) 50.0 μM, e) 0.1 mM, f) 0.5 mM, g) 1.0 mM, h) 5.0 mM and i) 10.0 mM KAuCl$_4$ acetonitrile solutions, respectively. Scale bars correspond to 2μm.

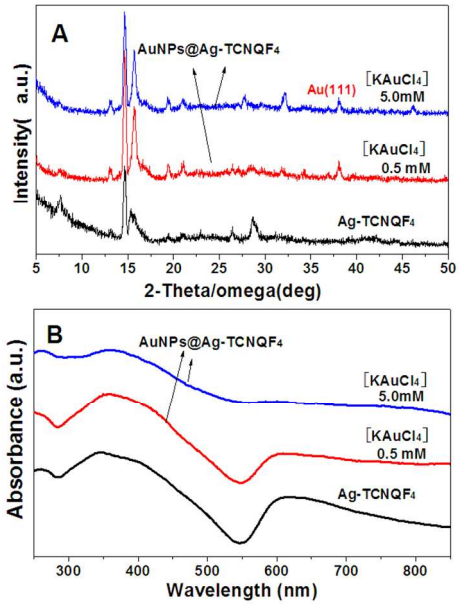

Figure 2. A) X-ray diffraction (XRD) patterns and B) Uv-vis absorption spectra of Ag-TCNQF$_4$ and AuNPs@Ag-TCNQF$_4$ which were prepared by using 0.5 and 5.0 mM KAuCl$_4$ solutions.

conjunction of Ag-TCNQF$_4$ crystal wires. As the KAuCl$_4$ concentration further increased, AuNPs became larger gradually and further covered the whole Ag-TCNQF$_4$ (Figures 1d-f). Besides, the diameter of AuNPs increased to 100 ~ 300 nm. The phenomenon of Ag-TCNQF$_4$ crystal wires dissolved in acetonitrile solutions was hardly observed at these conditions. When the concentration of KAuCl$_4$ arrived in 5.0 mM (Figure 1h), the Ag-TCNQF$_4$ crystal wires were partly etched into prolate ellipsoids because numerous Ag-TCNQF$_4$ were consumed in the presence of abundant Au salts. If much higher KAuCl$_4$ concentration was used, Ag-TCNQF$_4$ were totally destroyed and only AuNPs left (Figure 1i). So, the reaction between Ag-TCNQF$_4$ and KAuCl$_4$ in acetonitrile involves a competing reaction between the dissolution of Ag-TCNQF$_4$ and the redox based galvanic replacement process. The phenomenon consists with the reaction of CuTCNQ and KAuBr$_4$ in acetonitrile solutions.[21]

3.1.2 XRD analysis.

XRD patterns further confirmed the growth of AuNPs on the Ag-TCNQF$_4$ surface in this galvanic replacement reaction. Figure 2A is the XRD pattern of Ag-TCNQF$_4$, which displays that Ag-TCNQF$_4$ is in the space group C2/c with the lattice constants of a=13.35 Å, b=6.9 Å, c=25.725 Å, β=117°, and V=2111.43 Å, respectively. These data are in accordance with previous literature.[18] Ag-TCNQF$_4$ has stronger peaks (2θ) at 7.653 °, 13.168 °, 14.624 °, 15.353 °, 16.8 ° 26.52 ° and 26.79 °, corresponding to Ag-TCNQF$_4$ at (002, 200, 11-1, 004, 204, 400, 020), which are similar to the previous report.[11] According to Dunbar's report,[18] we can know that the obtained Ag-TCNQF$_4$ exhibits a single phase.

The XRD analysis of AuNPs@Ag-TCNQF$_4$ is also shown in Figure 2A. A strong peak (2θ) at 38.0 ° from a group of (111) planes in fcc structured Au was observed,[22] which confirms the formation of AuNPs on the Ag-TCNQF$_4$ crystal wires.

3.1.3 Uv-vis absorption analysis.

Figure 2B shows the Uv-vis absorption spectra of Ag-TCNQF$_4$ crystal wires and AuNPs@Ag-TCNQF$_4$ complexes. Ag-TCNQF$_4$ has two absorption peaks centered at around 357 and 630 nm, respectively. The 630 nm absorption band is originated from

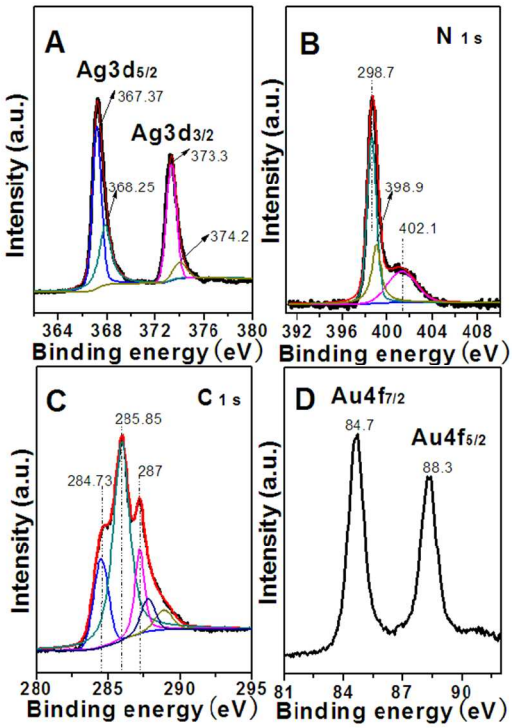

Figure 3. XPS spectra of Ag-TCNQF$_4$ in (A) Ag 3d, (B) N 1s and (C) C 1s regions, respectively. (D) XPS spectrum of AuNPs@Ag-TCNQF$_4$ in Au 4f region.

Table 1. The XPS assignments of elemental composition and chemical status of Ag-TCNQF$_4$ crystal wires on the Ag film.

Energy level	Binding energies (eV)	Area (P) CPS.eV	Assignment
Ag 3d$_{3/2}$	374.20	7771.703	Ag^0 [24,25]
	373.30	38529.67	Ag$^+$ in Ag-TCNQF$_4$
Ag 3d$_{5/2}$	368.25	33799.67	Ag^0
	367.37	52172.49	Ag$^+$ in Ag-TCNQF$_4$
N 1s	402.10	30351.21	shake-up processes of π-conjugated [26]
	398.68		anion TCNQF$_4^-$ in direct contact with Ag$^+$ and C≡N [26]
C 1s	284.73	145667.18	C=C[27]
	285.85		C≡N[27]
	287.00		fluorine/carbon binding[28]

TCNQF$_4$ radical anions and the 357 nm absorption band belongs to neutral Ag-TCNQF$_4$.[11] The Uv-vis absorption spectrum of AuNPs@Ag-TCNQF$_4$ prepared by using a 0.5 mM KAuCl$_4$ solution shows a decrease of the absorption intensity in 550-800 nm comparing to Ag-TCNQF$_4$. When the KAuCl$_4$ concentration was as high as 5.0 mM, the 630 nm peak became very weak, which is originated from the TCNQF$_4$ radical anions oxidized by KAuCl$_4$ solution during the galvanic replacement reaction. Meanwhile, a new absorption peak at 580 nm emerged, which is attributed to the LSP resonance band of AuNPs.

3.1.4 X-ray photoelectron spectroscopy analysis.

The elemental composition and chemical status of Ag-TCNQF$_4$ were analysis by XPS (Figure 3 A-C). Table 1 displays the elemental composition assignments. The XPS results prove the co-existence of Ag^0 and Ag-TCNQF$_4$ for the sample of Ag-TCNQF$_4$ crystal wires. The quantitative analysis was carried out according to the atomic sensitivity factors law.[23] The atomic ratio of Ag$^+$/N is nearly 1:4, proving that Ag$^+$ ions are coordinated to four TCNQF$_4^-$.[5] The atomic ratio of Ag$^+$/C is about 1:34.

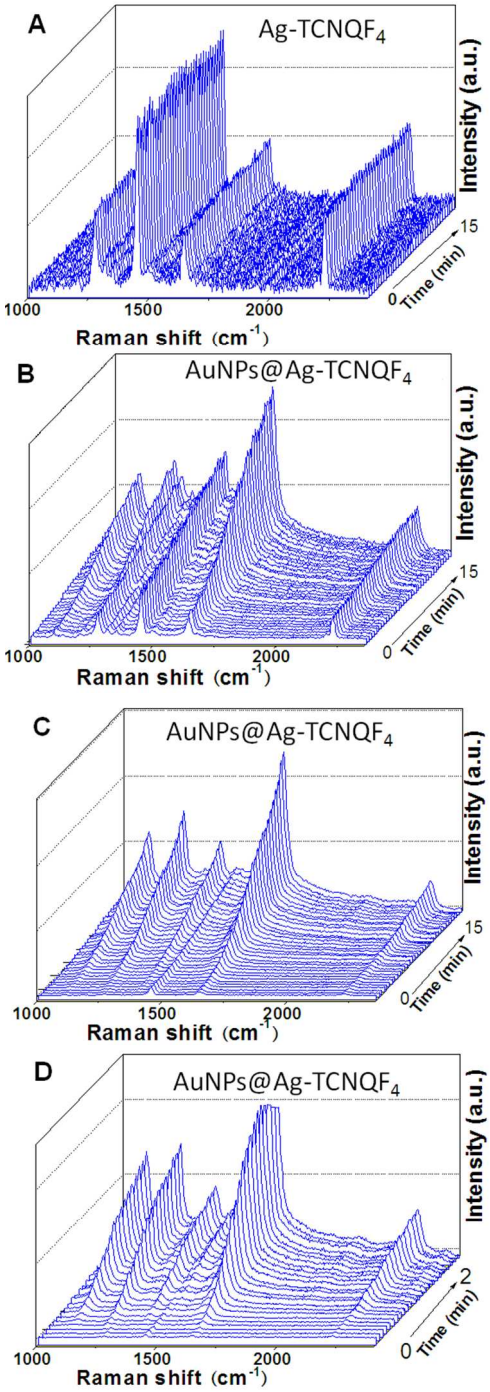

Figure 4. Time-resolved *in situ* Raman spectra of A)AgTCNQF$_4$ and AuNPs@AgTCNQF$_4$ which were prepared by using B)50.0 μM, C)0.5 mM and D)5 mM KAuCl$_4$ acetonitrile solutions under the photo-induced charge transfer reaction. The excitation wavelength was 532 nm.

Figure 3D shows the XPS spectrum of Au 4f region from the sample of AuNPs@Ag-TCNQF$_4$. The Au 4f energy values can be divided into 4f$_{7/2}$ and 4f$_{5/2}$ components. The major 4f$_{7/2}$ binding energy features at 84.7 eV, which is a characteristic energy of Au^0. [21] XPS further confirms the growth of AuNPs on the Ag-TCNQF$_4$ surface in this galvanic replacement reaction.

Table 2. Raman shift assignments of Ag-$TCNQF_4$ and Ag_2-$TCNQF_4$.

Raman shift of $TCNQF_4^-$(cm^{-1})		Raman shift of $TCNQF_4^{2-}$(cm^{-1})		Assignment
Experiment	Reference[12]	Experiment	Reference [a][12]	
2221(m)	2205(m)	2207-2259(m)	2135(m), 2175(m)	ν C≡N, δ C≡N
1638(s)	1641(s)	1642(s)	1648(s)	ν C=C ring
1446(s)	1443(s)	1390(s)	1428(w)	ν C-CN wing
		1240(m)	1242(w)	ν C-C wing, νC_6-C_1-C_7 deformation stretch
		1104(m)		νC_1-C_2-C_3 ring deformation stretch

ν, stretch; δ, bend; π, wagging; s, strong; w, weak; v, very; m, medium. [a] Data are from the previous paper for identification of $TCNQF_4$ redox level, whose donor are different from Ag_2-$TCNQF_4$.

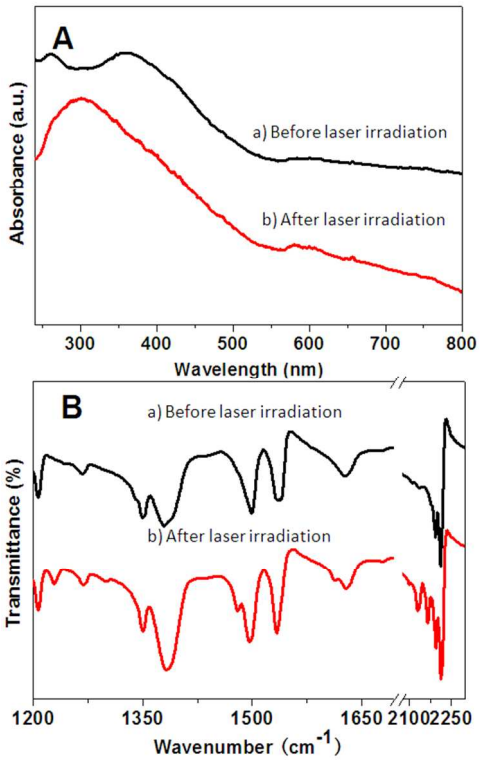

Figure 5. A) Uv-vis spectra and B) Infrared spectra of AuNPs@Ag-$TCNQF_4$ before (a) and after laser irradiation (b).

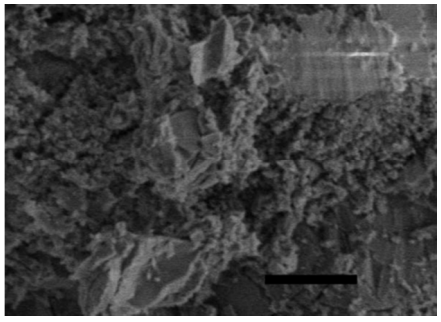

Figure 6. SEM of Ag_2-$TCNQF_4$ prepared by the photo-induced charge transfer from AuNPs@Ag-$TCNQF_4$. Scale bar is 5μm.

3.2 Photo-Induced Charge Transfer Process under Plasmon-Enhanced Catalysis

3.2.1 The formation of Ag_2-$TCNQF_4$.

As we stated previously that Ag-$TCNQF_4$ is a metal-organic charge transfer semiconductor, its photoelectrical property is very attractive. In this study, we also observed the phenomenon of photo-induced charge transfer happening on Ag-$TCNQF_4$ in presence of AuNPs. Importantly, we employed Raman spectroscopy to monitor and record this charge transfer process. Figures 4B, C and D present the time-resolved *in situ* Raman spectra of AuNPs@Ag-$TCNQF_4$ in a photo-induced charge transfer process. The excitation wavelength was 532 nm. For comparison, the time-resolved *in situ* Raman spectra of Ag-$TCNQF_4$ are provided (Figure 4A). Under the laser irradiation, the Raman signals of Ag-$TCNQF_4$ were unchanged within 15 min. Differently, with the laser irradiation, AuNPs@Ag-$TCNQF_4$ showed remarkable changes in Raman band intensities at 1642 (increase) and 1446 cm^{-1} (decrease) and in the emergence of new bands at 1390, 1240 and 1104 cm^{-1}. We attribute these changes to the formation of $TCNQF_4^{2-}$ under the existence of AuNPs.

Table 2 lists the Raman band assignments of Ag-$TCNQF_4$ and Ag_2-$TCNQF_4$ from Figure 4. To our knowledge, there is no literature displaying the Raman spectra of Ag_2-$TCNQF_4$. It might be because there are only two papers referring to success in synthesizing Ag_2-$TCNQF_4$.[16, 19] In present study, we infer that the product of the photo-induced charge transfer is Ag_2-$TCNQF_4$ via Raman band assignemnts (see ESI).

Therefore, this photo-induced charge transfer reaction can be expressed by Equation (3-6).

$$2\text{Ag-TCNQF}_4 \rightarrow \text{Ag-TCNQF}_4^+ + \text{Ag-TCNQF}_4^- \quad (3)$$

$$\text{Ag} \rightarrow \text{Ag}^+ + e^- \quad (4)$$

$$\text{Ag-TCNQF}_4^+ + e^- \rightarrow \text{Ag-TCNQF}_4 \quad (5)$$

$$\text{Ag-TCNQF}_4^- + \text{Ag}^+ \rightarrow \text{Ag}_2\text{-TCNQF}_4 \quad (6)$$

Semiconductor Ag-$TCNQF_4$ produces photon-generated electrons and holes under the laser irradiation.[29] The electrons from Ag on the bottom compensate above holes. Accordingly, the formed Ag^+ ions react with Ag-$TCNQF_4^-$ to form the Ag_2-$TCNQF_4$.

3.2.2 UV-vis, IR and SEM characterizations of AuNPs@Ag-$TCNQF_4$ before and after laser irradiation.

In order to further confirm the photo-induced product, the Uv-vis and IR spectra of AuNPs@Ag-$TCNQF_4$ before and after photo-induced charge transfer were measured (Figure 5). As we stated, before laser irradiation, a broad absorption between 280 and 545 nm (the maximal absorption wavelength is at 357 nm) attributing to the neutral Ag-$TCNQF_4$ was observed before 532 nm laser irradiation (curve a). After laser irradiation, the 357 nm band growing up (curve b). The new birth band is attributed to $TCNQF_4^{2-}$, which is consistent with the reported results.[12,19]

The IR spectra of AuNPs@Ag-$TCNQF_4$ before and after laser irradiation (Figure 5B) are in accord with the Uv-vis results. Compared with curve a, the C≡N stretching vibration modes at 2130 and 2165 cm^{-1} and the C=C ring stretch at 1477 and 1495

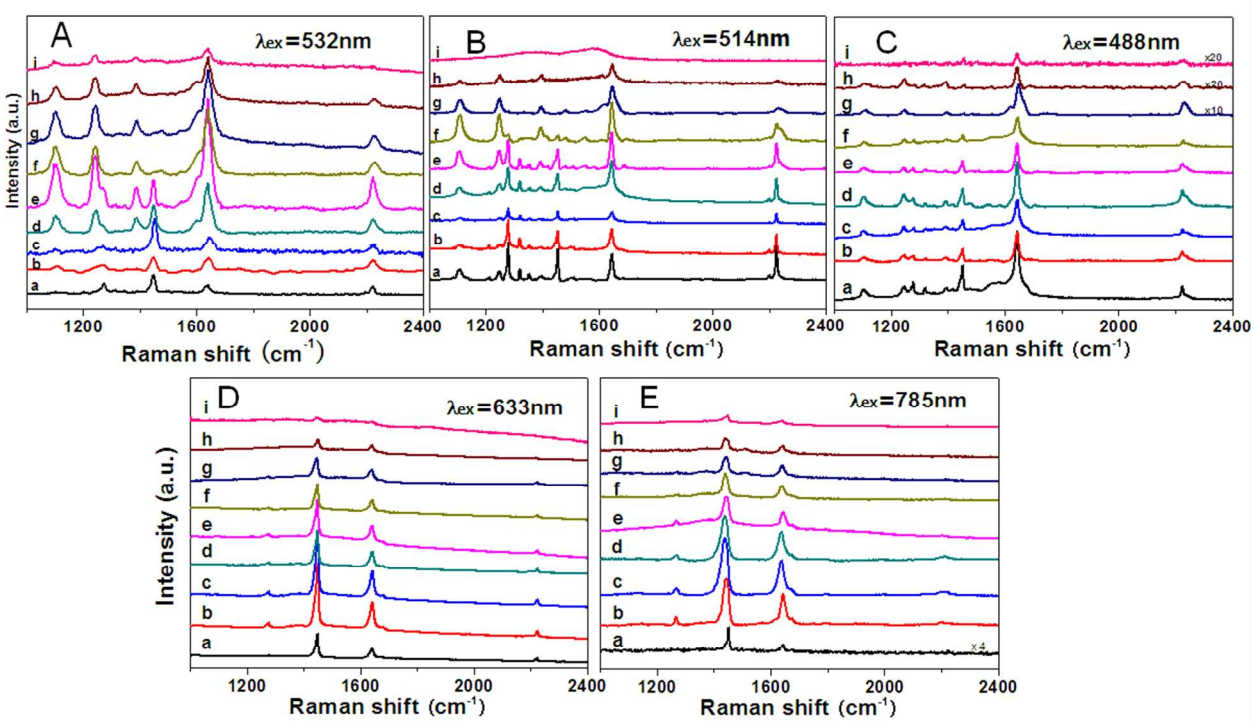

Figure 7. Raman spectra of a) Ag-TCNQF$_4$ crystal wires and AuNPs@Ag-TCNQF$_4$ prepared by using b) 1.0 μM , c)10.0 μM, d)50.0 μM, e)0.1 mM, f) 0.5 mM, g)1.0 mM, and h)5.0 mM $KAuCl_4$ solutions, respectively. The excitation wavelengths were A)532, B)514, C)488, D)633 and E)785nm, respectively.

cm^{-1} in curve b show shifts as a result of a increase of negative charges at symmetrical positions, suggesting the formation of TCNQF$_4^{2-}$.[19]

A SEM image of AuNPs@Ag-TCNQF$_4$ after photo-induced transformation is shown in Figure 6. We found that original crystal wires had been reduced and formed the amorphous Ag_2-TCNQF$_4$, which is accordance with provisions report [14]

3.2.3 The influence of the loading of AuNPs on photo-induced charge transfer process.

It also can be inferred from Figure 4 that with the coverage of AuNPs increasing, the reaction rate increases. In Figures 4B and 4C, it experienced 20 and 15 min to reach the equilibrium of the charge transfer process. For AuNPs@Ag-TCNQF$_4$ prepared by using 5.0 mM of $KAuCl_4$, the photo-induced charge transfer process arrived in equilibrium just within 2 min (Figure 4D).

Figure 7 A-C shows the Raman spectra of Ag-TCNQF$_4$ crystal wires (curve a) and AuNPs@Ag-TCNQF$_4$ with different coverages of Au NPs (from curve b-i, the coverage density increases) under different excitation wavelengths invovling 488, 514 and 532 nm, respectively. Comparing curve b-i, we can find that the ratio of peak intensity (1390 cm^{-1} / 1446 cm^{-1}) increases, which indicates the degree of charge transfer from TCNQF$_4^-$ to TCNQF$_4^{2-}$ is ascent. These results reflect Au NPs play an active action in the photo-induced charge transfer process. For the AuNPs@Ag-TCNQF$_4$ with more Au deposition (curve f-i in Figures 6a-c), the LSPR absorption of Au become dominating, weakening Raman signals consequently.

3.2.4 The influence of laser wavelength on photo-induced charge transfer process.

Moreover, this photo-induced charge transfer process from TCNQF$_4^-$ to TCNQF$_4^{2-}$ is dependent on excitation photonic energy. Figure 6 displays the laser wavelength effect on the Raman spectra of Ag-TCNQF$_4$ crystal wires (curve a) and AuNPs@Ag-TCNQF$_4$ (cureves b-i). AuNPs@Ag-TCNQF$_4$ exhibited different photoelectrical property under different lasers irradiation. Under 532 nm laser, new bands corresponding to TCNQF$_4^{2-}$ can be identified (curve b-i in Figures 7A). Similar changes can be found under the excitation wavelengths of 514 and 488 nm (Figures 7B and C). The Raman peak changes were unobserved when using 633 nm as excitation wavelength (curve b-i in Figure 7D). Raman data obtained at 785 nm excitation prove again that no new band emerged (curve b-i in Figure 7E). These results imply that the higher energy lasers can cause an electron transfer reaction, resulting in formation of TCNQF$_4^{2-}$. The photo-induced charge transfer process only happens when the irradiation energy is over 2.33 eV (532 nm).

Table 3. The reaction time for completing the photo-induced charge transfer reaction in AuNPs@Ag-TCNQF$_4$ under different power densities.

Power density ($\times 10^5$ W/cm^2)	Reaction Time (min)
3.87	45.0
7.63	9.0
10.1	5.0
12.7	1.0
14.6	0.5
17.9	0.3
22.1	0.21
24.5	0.20

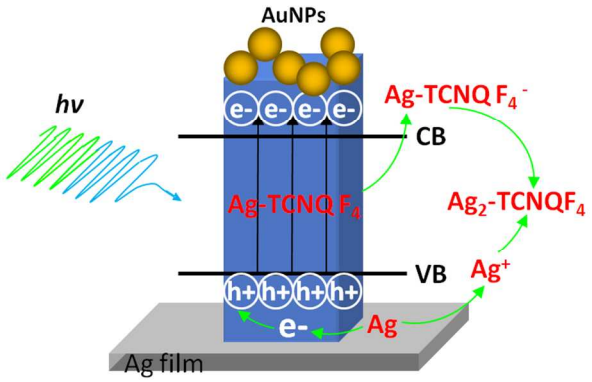

Scheme 2.The mechanism of the photo-induced charge transfer reaction in AuNPs@Ag-$TCNQF_4$.

3.2.5 The influence of power density on photo-induced charge transfer process.

In addition, power density also has influence on the Ag-$TCNQF_4$ transformation process. We measured the reaction time for the complete transformation from $TCNQF_4^-$ to $TCNQF_4^{2-}$ under different power densities (532 nm laser). Table 3 shows the reaction finishing time under different power density. With the laser power density increasing, the reaction time for complete transformation decreases.

3.3. The Mechanism of Photo-Induced Charge Transfer Process under Plasmon-Enhanced Catalysis

Based on the above results, we propose the mechanism of the photo-induced charge transfer process (Scheme 2). Owing to AuNPs have strong visible-light absorption due to surface plasmon resonances,[30] the light absorption on AuNPs@Ag-$TCNQF_4$ has been enhanced for photo-catalysis, resulting in a high reation rate of charge transfer from $TCNQF_4^-$ to $TCNQF_4^{2-}$. Ag-$TCNQF_4$ has a work function of 1.07 eV,[13] which is lower than the work function of Au (5.2 eV).[31] So electrons can be extracted from the semiconductor (Ag-$TCNQF_4$) to Au (see Equation 3).[32] The details of this effect process are illustrated in Scheme 2. First, an incident photon interacts with electrons in the valence band of Ag-$TCNQF_4$, promoting them across the band gap to the conduction band.[33] AuNPs deposited on semiconductor surface form the Schottky barriers at the interface of Au/semiconductor, which makes electrons continuous transfer from semiconductor to metal and further collect at the Au/semiconductor interface.[21] The existence of AuNPs is favorable for suppressing electron/hole recombination. The holes are diffused to the surface of Ag-$TCNQF_4$. As a result, Ag atoms from the bottom Ag film compensate electrons for holes. The superfluous electrons at the Au/semiconductor interface return to semiconductor and reduce Ag-$TCNQF_4$ to produce Ag-$TCNQF_4^-$ instead of the recombination with hole. Due to the large difference in the chemical potential of the bottom Ag and the top Ag-$TCNQF_4$ crystals, the migration of Ag^+ ions along the semiconductor crystal will be facilitated. Therefore, the fast migration of Ag^+ ions react with the photo-generated Ag-$TCNQF_4^-$, forming Ag_2-$TCNQF_4$.[23]

However, we found Ag_2-$TCNQF_4$ could revert back to Ag-$TCNQF_4$ under several hours storage in dark. Previous paper also reported that the transformation of Ag_2-$TCNQF_4$ to metallic Ag and Ag-$TCNQF_4$ when exposing a Ag_2-$TCNQF_4$ thin film to a low-power visible laser.[19] We suppose there is a competing reversible reaction between Ag_2-$TCNQF_4$ and Ag-$TCNQF_4$. When a higher energy visible laser irradiates Ag-$TCNQF_4$, with the AuNPs as a catalyst, the reaction goes to forming Ag_2-$TCNQF_4$. It is a fast transformation process. When the laser energy is removed, it can be reverse back to Ag-$TCNQF_4$, which is a slow process.

4. Conclusions

A plasmon-catalyzed transformation from Ag-$TCNQF_4$ to Ag_2-$TCNQF_4$ was observed, when they were excited at 532 nm (2.33 eV) or more high energy lasers. The degree and the rate of charge transfer occurring on Ag-$TCNQF_4$ relied on the excitation wavelength, excitation intensity, the irradiation time and the coverage density of Au NPs. This study puts forward a possible approach to synthesize Ag_2-$TCNQF_4$ controllably via photo-transformation. In addition, it provides a good model to study the charge transfer process in metal/semiconductor systems. The reaction between Ag_2-$TCNQF_4$ and Ag-$TCNQF_4$ is reversible, which make AuNPs@Ag-$TCNQF_4$ be a potential candidate for an erasable memory storage material. Relative study is still under going.

5. Acknowledgments

This work was supported by the National Natural Science Foundation of China (91027010 and 21073073) and National Instrumentation Program of the Ministry of Science and Technology of China no. 2011YQ03012408. We appreciate Prof. John R. Lombardi, Department of Chemistry, City College of New York and Prof. Dejun Wang, Jilin University for helpful discussion.

6. Notes and references

[a] *State Key Laboratory of Supramolecular Structure and Materials, Jilin University, 2699 Qianjin Ave., Changchun 130012, P. R. China Tel: +86-431-85168505; Fax: +86-431-85193421; *Email: xusp@jlu.edu.cn*
[b] *State Key Laboratory of Theoretical and Computational Chemistry, Jilin University, 2 Liutiao Road, Changchun 130023, P. R. China.*

† Electronic Supplementary Information (ESI) available: Experimental and calculated Raman Spectra of $TCNQF_4$, Ag-$TCNQF_4$ and Ag_2-$TCNQF_4$. See DOI: 10.1039/b000000x/

1. K. B. Zheng, X. Y. Li, X. L. Mo, G. Y. Chen, Z. D. Wang and G. R. Chen, *Appl. Surf. Sci.*, 2010, **256**, 2764–2768.
2. Ch. Muller, D. Deleruyelle, R. Muller, M. Thomas, A. Demolliens, Ch. Turquat and S. Spiga, *Solid-State Electron.*, 2011, **56**, 168–174.
3. C. N. Ye, G. Y. Cao, K. B. Zheng and G. R. Chen, *J. Phys. Conference Series.*, 2011, **276**, 012198.
4. J. A. Freire, G. A. Dal Moro and R. Toniolo, *Org. Electron.*, 2006, **7**, 379–402.
5. C. N. Ye, G. Y. Cao, F. Fang, H. H. Xu, X. Y. Xing, D. L. Suna and G. R. Chen, *Micron.*, 2005, **36**, 461–464.
6. G. Y. Cao and G. R. Chen, *Micron.*, 2005, **36**, 285–290.
7. H. B. Liu, Z. L. Wang and D. B. Zhu, *Nanotechnology*, 2007, **18**, 495–704.
8. J. C. Xiao, H. Zhang and Q. C. Zhang, *Small,* 2011, **7**, 1242–1246.
9. C. Zhao and A. M. Bond, *J. Am. Chem. Soc.*, 2009, **131**, 4279–4287.

10. L. Ren, L. Fu, Y. W. Liu, S. Q. Chen and Z. F. Liu, *Adv. Mater.*, 2009, 21, 4742–4746.
11. K. Xiao, A. J. Rondinone, A. A. Puretzky, I. N. Ivanov, S. T. Retterer and B. G. David, *Chem. Mater.*, 2009, **21**, 4275–4281.
12. T. H. Le, A. M. Bond and L. L. Martin, *Inorg. Chim. Acta.,* 2013, **395**, 252-254.
13. K. Xiao, M. N. Yoon, A. J. Rondinone, E. A. Payzant and D. B. Geohegan. *J. Am. Chem. Soc.*, 2012, **134**, 14353−14361.
14. T. H. Le, A. P. O'Mullane, L. L. Martin and A. M. Bond. *J. Solid State Electrochem.*, 2011, **15**, 2293–2304.
15. C. B. Ouyang, Y. B. Guo, H. B. Liu, Y. J. Zhao, G. X. Li, Y. Y. Li, Y. L. Song and Y. L. Li, *Journal of Physical Chemistry C*, 2009, **113**, 7044–7051.
16. M. Mahajan, S. K. Bhargava and A. P. O'Mullane, *RSC Advances.*, 2013, **3**, 4440–4446.
17. R. S. Potember, T. O. Poehler, A. Rappa, D. O. Cowan and A. N. Bloch, *Synth Met.*, 1982, **4**, 371–380.
18. S. A. O'Kane, R. Clerac, H. H. Zhao, X. Ouyang, J. R. Galan-Mascaros, R. Heintz and K. R. Dunbar. *J. Solid State Chem.*, 2000, **152**, 159–173.
19. A. M. Kotsiliou and W. M. Risen, *Solid State Commun.*, 1988, **68**, 503–505.
20. B. Mukherjee, M. Mukherjee, J. Park and S. Pyo, *J. Phys. Chem. C*, 2010, **114**, 567–571.
21. A. Pearson, A. P. O'Mullane, V. Bansal and S. K. Bhargava, *Inorg. Chem.*, 2011, **50**, 1705–1712.
22. A. P. O'Mullane, S. J. Ippolito, Y. M. Sabri, V. Bansal and S. K. Bhargava, *Langmuir*, 2009, **25**, 3845–3852.
23. C. D. Wagner, L. E. Davis, M. V. Zeller, J. A. Taylor, R. H. Raymond and L. H. Gale, *Surf. Interface Anal.*, 1981, **3**, 211–225.
24. P. Wang, B. B. Huang, Z. Z. Lou, X. Y. Zhang, X. Y. Qin, Y. Dai, Z. K. Zheng and X. N. Wang, *Chem.-Eur. J.*, 2010, **16**, 538−544.
25. L. Han, P. Wang, C. Z. Zhu,; Y. M. Zhai and S. J. Dong, *Nanoscale*, 2011, **3**, 2931−2935.
26. W. Chen, D. C. Qi, X. Y. Gao and A. T. S. Wee, *Prog. Surf. Sci.*, 2009, **84**, 279–321.
27. D. W. Zeng, K. C. Yung and C. S. Xie, *Surf. Coat. Tech*., 2002, **153**, 210–216.
28. G. Nansé, E. Papirer, P. Fioux, F. Moguet and A. Tressaud, *Carbon.*, 1997, **35**, 175–194.
29. K. Woan, G. Pyrgiotakis and W. Sigmund, *Adv. Mater.*, 2009, **21**, 2233–2239.
30. C. H. An, R. P. Wang, S. T. Wang and X. Y. Zhang, *J. Mater. Chem.*, 2011, **21**, 11532−11536.
31. W. M. H. Sachtler, G. J. H. Dorgelo and A. A. Holscher, *Surf.Sci.*, 1966, **5**, 221–229.
32. L. Linsebigler, G. Lu and J. T. Yates, *Chem. Rev.*, 1995, **95**, 735–758.
33. E. Thimsen, F. Le. Formal, M. Grätzel and S. C. Warren, *Nano Lett.*, 2011, **11**, 35–43.
34. H. X. Ji, J. S. Hu, Y. G. Guo, W. G. Song and L. J. Wan, *Adv. Mater.*, 2008, **20**, 4879–4882.